Large amplitude internal solitary waves in a two-layer system of piecewise linear stratification

Arnaud Goullet and Wooyoung Choi[a)]
Department of Mathematical Sciences, Center for Applied Mathematics and Statistics, New Jersey Institute of Technology, Newark, New Jersey 07102-1982, USA

(Received 15 April 2008; accepted 10 August 2008; published online 16 September 2008)

We study large amplitude internal solitary waves in a two-layer system where each layer has a constant buoyancy frequency (or Brunt–Väisälä frequency). The strongly nonlinear model originally derived by Voronovich [J. Fluid Mech. **474**, 85 (2003)] under the long wave assumption for a density profile discontinuous across the interface is modified for continuous density stratification. For a wide range of depth and buoyancy frequency ratios, the solitary wave solutions of the first two modes are described in detail for both linear-constant and linear-linear density profiles using a dynamical system approach. It is found that both mode-1 and mode-2 solitary waves always point into the layer of smaller buoyancy frequency. The width of mode-1 solitary waves is found to increase with wave amplitude while that of mode-2 solitary waves could decrease. Mode-1 solitary wave of maximum amplitude reaches the upper or lower wall depending on its polarity. On the other hand, mode-2 solitary wave of maximum amplitude can reach the upper or lower wall only when the interface is displaced toward the shallower layer; otherwise, the maximum wave amplitude is smaller than the thickness of the deeper layer. Streamlines and various physical quantities including the horizontal velocity and the Richardson number are computed and discussed in comparison with the recent numerical solutions of the Euler equations by Grue *et al.* [J. Fluid Mech. **413**, 181 (2000)]. © *2008 American Institute of Physics*. [DOI: 10.1063/1.2978205]

I. INTRODUCTION

Nonlinear internal solitary waves have been observed frequently in density stratified coastal oceans for many years, but recent field measurements of exceptionally large amplitude solitary waves have prompted a number of new theoretical studies, which have improved greatly the understanding of highly nonlinear internal solitary wave characteristics.

For continuous density profiles, steady solitary wave solutions of the Euler equations (in a frame of reference moving with the solitary wave) can be obtained by solving numerically the Dubreil–Jacotin–Long (DJL) equation.[1,2]

Among many, Tung *et al.*,[3] Turkington *et al.*,[4] and Brown and Christie[5] computed large amplitude mode-1 and mode-2 solitary wave solutions. It was shown that, as the wave amplitude increases, the characteristic wavelength of solitary waves increases so that flat "tabletop" solitary wave solutions can be found. In the presence of background shear, Stastna and Lamb[6] computed the solitary wave solutions of the DJL equation using the variational method of Turkington *et al.*[4]

Due to their simplicity, the reduced long wave models such as the Korteweg–de Vries (KdV) and the extended KdV equations[7,8] have been widely used, but these classical weakly nonlinear models are not applicable to the large amplitude regime of interest. For a system of two constant density layers, strongly nonlinear long wave models have been proposed and studied by Miyata[9] and Choi and Camassa[10] for both shallow and deep configurations. Compared to the numerical solutions of the Euler equations, the strongly nonlinear models predict accurately the wave profiles and the associate velocity fields of large amplitude internal solitary waves. Recently, Camassa *et al.*[11] showed that the solitary wave solutions of the strongly nonlinear models are in good agreement with laboratory experiments of Grue *et al.*[12] for the shallow configuration and those of Michallet and Barthélemy[8] for the deep configuration. Since the characteristic horizontal length scale increases with wave amplitude, it is not so surprising that the long wave model approximates better as the wave amplitude increases. It is therefore quite an accurate statement that the usefulness of these strongly nonlinear long wave models has been well recognized for large amplitude internal solitary waves.

For real oceanic applications, the assumption of constant density layers could be inaccurate and it would be necessary to consider more realistic density profiles. A density profile that is more realistic, but simple enough so that any analytical description is feasible is a linear density profile with a constant Brunt–Väisälä (or buoyancy) frequency for which the nonlinear Euler equations can be reduced to the linear Helmholtz equation for the stream function. By approximating a realistic density profile by a number of layers of different constant buoyancy frequencies, the Helmholtz equation can be easily solved in each layer although two neighboring layers are coupled nonlinearly through the boundary conditions at the interfaces. For two and three layer systems, Grue *et al.*[13] and Fructus and Grue,[14] respectively, adopted a boundary integral formulation to compute numerically fully nonlinear solutions of the Euler equations. On the other hand, Voronovich[15] used a long wave asymptotic approach

[a)]Electronic mail: wychoi@njit.edu.

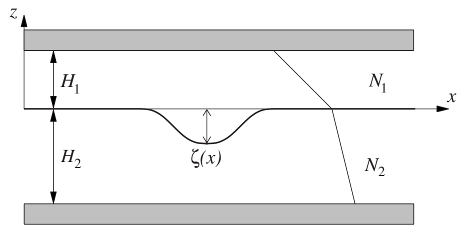

FIG. 1. Two-layer system of piecewise linear density profile.

similar to that of Choi and Camassa[10] and obtained a strongly nonlinear (steady) model for a two-layer system of constant buoyancy frequencies. In his work, Voronovich[15] allowed a density jump across the interface where continuity of pressure and normal velocity is required. For a set of physical parameters for the Coastal Ocean Probing Experiment (COPE) experiment,[16] it was shown that the solitary wave solutions of Voronovich's model are in reasonable agreement with the observed data, but no systematic description of solitary wave characteristics for a wide range of physical parameters involved was provided.

In this paper, we modify the approach of Voronovich[15] such that the density is continuous across the interface although the slope of density profile (or the Brunt–Väisälä frequency) is assumed to have a jump. Due to the absence of density jump, the interface is no longer considered a vortex sheet and, therefore, continuity of tangential and normal velocities must be the boundary conditions at the interface, which are different from those of Voronovich.[15] With the long wave model presented in Sec. II, both mode-1 and mode-2 solitary wave solutions are obtained by solving a system of coupled nonlinear ordinary differential equations. A simpler density profile of linear and constant density stratification in the upper and lower layers, respectively, is considered first in Sec. III. The characteristics of large amplitude internal solitary waves are described in detail and the corresponding streamlines and other flow quantities are also presented. Solitary wave solutions for the linear-linear density stratification are then discussed in Sec. IV.

II. MATHEMATICAL MODEL

We consider a system of two fluid layers where the density is a piecewise linear function so that it can be expressed as

$$\rho(z)=\begin{cases}\rho_0(1-N_1^2 z/g) & \text{for } 0\le z\le H_1,\\ \rho_0(1-N_2^2 z/g) & \text{for } -\mathrm{H}_2\le z\le 0,\end{cases} \tag{1}$$

where $N_i>0$ are the Brunt–Väisälä (or buoyancy) frequencies that are assumed to be constant in each layer, H_i are the layer thickness, ρ_0 is the density at the interface, and g is the gravitational acceleration. See Fig. 1 for a schematic of the problem. Notice that the density is continuous, but its slope has a jump across the interface located initially at $z=0$.

To describe a traveling wave propagating with constant speed c in the negative x-direction, we adopt a frame of reference moving with the wave so that the problem is steady and the total stream function, Ψ_i, can be written as

$$\Psi_i(x,z)=cz+\psi_i(x,z), \tag{2}$$

where ψ_i are the stream functions representing by the internal wave motion and $\psi_i(x,z)\to 0$ as $x\to-\infty$ is imposed at the upstream. After assuming that the fluid is incompressible and inviscid, the Euler equations can be reduced, under the Boussinesq approximation, to the DJL equation[1,2] for ψ_i,

$$\frac{\partial^2\psi_i}{\partial x^2}+\frac{\partial^2\psi_i}{\partial z^2}+\frac{N_i^2}{c^2}\psi_i=0 \quad \text{for} \quad i=1,2. \tag{3}$$

Since N_i are assumed to be constant in each layer, Eq. (3) is the Helmholtz equation. The boundary conditions at the upper and lower rigid boundaries are given by

$$\psi_1=0 \quad \text{at} \quad z=H_1, \quad \psi_2=0 \quad \text{at} \quad z=-H_2, \tag{4}$$

while the kinematic boundary conditions at the interface located at $z=\zeta(x)$ are given, for both $i=1$ and 2, by

$$c\zeta_x+\psi_{i,z}\zeta_x+\psi_{i,x}=0 \quad \text{at} \quad z=\zeta(x). \tag{5}$$

where the subscripts x and z represent partial derivatives. Notice that subtracting these two kinematic boundary conditions $(i=1,2)$ from each other gives continuity of normal velocity, or, equivalently, continuity of stream function across the interface,

$$\psi_1=\psi_2 \quad \text{at} \quad z=\zeta(x). \tag{6}$$

In addition, since the density is assumed to be continuous at the interface, no velocity jump is allowed across the interface. This requirement is fulfilled by continuity of horizontal velocity

$$\psi_{1,z}=\psi_{2,z} \quad \text{at} \quad z=\zeta(x), \tag{7}$$

which, along with Eq. (6), guarantees continuity of normal and tangential velocities across the interface and, therefore, continuity of pressure (see Appendix A).

Using the long wave approximation for small H_i/λ, where λ is the characteristic wavelength, the solution of Eq. (3) correct to $O(H_i^2/\lambda^2)$ can be found,[15] after imposing the boundary conditions given by Eqs. (4) and (5), as

$$\begin{aligned}\psi_i(x,z)=&-c\zeta\frac{\sin\left(\frac{N_i(z-z_i)}{c}\right)}{\sin\left(\frac{N_i(\zeta-z_i)}{c}\right)}+\frac{c^3}{2N_i^2}\left[\frac{\zeta}{\sin\left(\frac{N_i(\zeta-z_i)}{c}\right)}\right]_{xx}\\ &\times\left[\frac{N_i(\zeta-z_i)}{c}\cot\left(\frac{N_i(\zeta-z_i)}{c}\right)\sin\left(\frac{N_i(z-z_i)}{c}\right)\right.\\ &\left.-\frac{N_i(z-z_i)}{c}\cos\left(\frac{N_i(z-z_i)}{c}\right)\right],\end{aligned} \tag{8}$$

where $z_1=H_1$ and $z_2=-H_2$. The first term of Eq. (8) is the solution of $\psi_{i,zz}+(N_i^2/c^2)\psi_i=0$ that is the leading-order approximation of Eq. (3) for long waves and the remaining terms are the next-order corrections at $O(H_i^2/\lambda^2)$.

Notice that when linearized for $\zeta/H_i\ll 1$, the first term of Eq. (8) becomes the linear long wave solution for ψ_i,

$$\psi_1^{\text{linear}} \sim \frac{\sin[N_1(H_1 - z)/c]}{\sin(N_1H_1/c)},$$
$$\psi_2^{\text{linear}} \sim \frac{\sin[N_2(H_2 + z)/c]}{\sin(N_2H_2/c)}. \tag{9}$$

By imposing the remaining boundary condition given by Eq. (7), the equation for the interface $\zeta(x)$ can be obtained, with an error of $O(H_i^2/\lambda^2)$, as

$$A(\zeta)\zeta_{xx} + B(\zeta)\zeta_x^2 + C(\zeta) = 0, \tag{10}$$

where

$$A(\zeta) = \frac{1}{4N_1}\csc^2\left(\frac{N_1(H_1-\zeta)}{c}\right)\left[c + N_1\zeta \cot\left(\frac{N_1(H_1-\zeta)}{c}\right)\right]\left[c \sin\left(\frac{2N_1(H_1-\zeta)}{c}\right) - 2N_1(H_1-\zeta)\right]$$
$$+ \frac{1}{4N_2}\csc^2\left(\frac{N_2(H_2+\zeta)}{c}\right)\left[c - N_2\zeta \cot\left(\frac{N_2(H_2+\zeta)}{c}\right)\right]\left[c \sin\left(\frac{2N_2(H_2+\zeta)}{c}\right) - 2N_2(H_2+\zeta)\right], \tag{11}$$

$$B(\zeta) = \frac{1}{8c}\csc^4\left(\frac{N_1(H_1-\zeta)}{c}\right)\left[c \sin\left(\frac{2N_1(H_1-\zeta)}{c}\right) - 2N_1(H_1-\zeta)\right] \times \left[N_1\zeta\left\{3 + \cos\left(\frac{2N_1(H_1-\zeta)}{c}\right)\right\}\right.$$
$$\left. + 2c \sin\left(\frac{2N_1(H_1-\zeta)}{c}\right)\right] + \frac{1}{8c}\csc^4\left(\frac{N_2(H_2+\zeta)}{c}\right)\left[c \sin\left(\frac{2N_2(H_2+\zeta)}{c}\right) - 2N_2(H_2+\zeta)\right]$$
$$\times \left[N_2\zeta\left\{3 + \cos\left(\frac{2N_2(H_2+\zeta)}{c}\right)\right\} - 2c \sin\left(\frac{2N_2(H_2+\zeta)}{c}\right)\right], \tag{12}$$

$$C(\zeta) = \zeta\left[N_1 \cot\left(\frac{N_1(H_1-\zeta)}{c}\right) + N_2 \cot\left(\frac{N_2(H_2+\zeta)}{c}\right)\right]. \tag{13}$$

We stress that continuity of horizontal velocity (or, equivalently, tangential velocity) across the interface is imposed in this paper and the coefficients of Eq. (10), A, B, and C, are different from those of Voronovich.[15] In Ref. 15 a density jump across the interface is introduced which allows a jump in tangential velocity induced by the baroclinic vorticity generation mechanism and, therefore, only continuity of pressure is required. While continuity of normal and tangential velocities implies continuity of pressure, the converse is not necessarily true (see Appendix A).

By introducing $(q,p) \equiv (\zeta, \zeta_x)$, Eq. (10) can be rewritten as the following system of ordinary differential equations:

$$\dot{q} = p, \quad \dot{p} = -\frac{B(q)p^2 + C(q)}{A(q)}, \tag{14}$$

where the dot denotes differentiation with respect to x. Notice that the origin $(q,p)=(0,0)$ is always a fixed point due to the boundary conditions at infinities for solitary waves. Furthermore, for solitary wave solutions to exist, the origin in phase space (q,p) has to be a saddle point connected to itself by a homoclinic orbit. The condition on the Jacobian for a saddle point to exist at the origin is given by $C'(0)/A(0) < 0$ (Ref. 15) that can be rewritten as

$$\frac{N_1 \cot(N_1H_1/c) + N_2 \cot(N_2H_2/c)}{c[cN_2 \cot(N_1H_1/c) + cN_1 \cot(N_2H_2/c) - N_1N_2\{H_1 \csc^2(N_1H_1/c) + H_2 \csc^2(N_2H_2/c)\}]} < 0. \tag{15}$$

To find solitary wave solutions numerically, the system is integrated, using a standard fourth-order Runge–Kutta method, along a homoclinic orbit. The initial condition on the unstable manifold is chosen to be close, of the order of 10^{-8}, to the origin and is found from the eigenvectors with positive real eigenvalues of the linearized system of Eq. (14).

For a given set of parameters,

$$H \equiv H_2/H_1, \quad N \equiv N_2/N_1, \tag{16}$$

inequality (15) determines the admissible ranges of wave speed c, as illustrated by the shaded regions in Fig. 2,

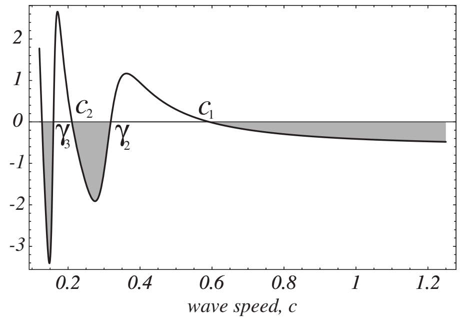

FIG. 2. Admissible range of wave speed c (shaded region) for a saddle point to appear at the origin for $H=5$ and $N=0.2$.

$$c \geq c_1 \quad \text{for mode } 1,$$
$$c_m \leq c \leq \gamma_m \quad \text{for mode} \quad m=2,3,\ldots. \tag{17}$$

Notice that Fig. 2 is qualitatively similar to Fig. 1(a) in Voronovich[15] although the coefficients of the equation for the interface are different, as mentioned previously. In Eq. (17), c_m $(m=1,2,\ldots)$ are the linear long wave speeds that are the zeros of the numerator of Eq. (15) in descending order of magnitude,

$$N_1 \cot(N_1H_1/c_m) + N_2 \cot(N_2H_2/c_m) = 0, \tag{18}$$

while γ_m $(m=2,3,\ldots)$ are the singularities of the denominator of Eq. (15), i.e.,

$$\sin(N_iH_i/\gamma_m) = 0 \quad \text{for} \quad i=1,2, \tag{19}$$

in descending order. Notice that the condition given by Eq. (15) is necessary, but not sufficient, and solitary wave solutions exist only on subintervals of the admissible speed range.

Hereafter, to fix the length and time scales, we choose $H_1=1$ and $N_1=1$. Then, $H_2=H$ and $N_2=N$ represent the depth and buoyancy frequency ratios, respectively. In this paper, we discuss solitary wave solutions for the following two different density profiles: linear-constant (case 1) and linear-linear (case 2) density profiles. Although case 1 can be recovered from case 2 with $N=0$, it is considered separately to make our discussion more accessible.

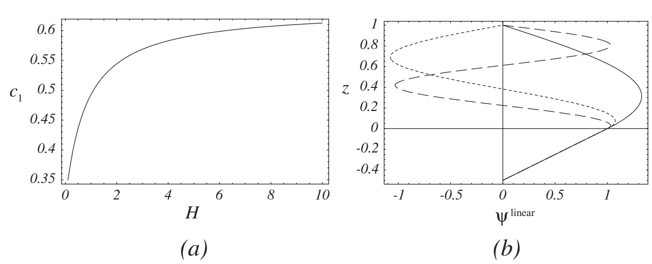

FIG. 3. (a) Linear long wave speed of first mode, c_1, vs depth ratio, H, for $N=0$. (b) Linear eigenfunctions (ψ) for mode 1 (—), mode 2 (- - -), and mode 3 (— —) for $N=0$ and $H=0.5$.

III. CASE 1: LINEAR-CONSTANT DENSITY PROFILE

When the density of the lower layer is constant $(N=0)$, the thickness of the lower layer (or the depth ratio) H is the only physical parameter. Then, for a fixed depth ratio, the linear long wave speed c_m can be found by solving Eq. (18). For example, the linear long wave speeds for the first four modes can be found as $(c_1,c_2,c_3,c_4)=(0.437,0.197,0.124,0.090)$, $(0.493, 0.204, 0.125, 0.090)$, and $(0.592, 0.210, 0.127, 0.091)$ for $H=0.5$, 1, and 5, respectively. For these depth ratios, notice that the wave speeds increase with H although the wave speeds for the higher modes are not so different. Mode-1 linear long wave speed c_1 for varying H is shown in Fig. 3(a). For $H=0.5$, the first three linear eigenfunctions given by Eq. (9) with $\psi_2^{\text{linear}}=(H_2+z)/H_2$ are shown in Fig. 3(b).

Mode-1 and mode-2 internal waves are most commonly observed in field and laboratory experiments[17–19] and we therefore limit our detailed discussion of solitary waves to the first two modes. Recently, for case 1, Grue *et al.*[13] computed mode-1 solitary wave solutions of the Euler equations numerically using a boundary integral method and compared them with their own laboratory experiment. Here, whenever possible, mode-1 solitary wave solutions of the long wave model are discussed in comparison with their numerical solutions. On the other hand, to the best of our knowledge, no systematic parameter study for mode-2 solitary waves is available for a two-layer system of piecewise linear stratification except for mode-2 periodic waves for a two-layer system of constant densities in Refs. 20 and 21 and no comparison of mode-2 solitary wave solutions with previous results is presented.

A. Mode-1 solitary waves

For a two-layer system of linear-constant density stratification, as described in Appendix B, mode-1 internal solitary waves always point into the layer of constant density and, regardless of depth ratio, only solitary waves of depression (negative polarity) exist. This is consistent with what Grue *et al.*[13] observed numerically. In contrast, for a two-layer system of constant densities, the polarity of solitary waves depends on depth and density ratios: for example, if the density ratio is close to 1, the interface is displaced toward the deeper layer.

For case 1, mode-1 internal solitary waves of depression exist over the following speed range:

$$c_1 \leq c \leq \gamma_1, \quad \gamma_1 = (1+H)/\pi. \tag{20}$$

Figure 4 shows homoclinic orbits in phase space (q,p), as defined in Eq. (14), and the corresponding solitary wave profiles for three different wave speeds, $c=(0.8,1.6,1.909)$, and a depth ratio of $H=5$. Unlike a two-layer system of constant densities where no solitary wave solution exists beyond the maximum wave amplitude that is always smaller than the thickness of either layer, the maximum speed solitary wave of depression reaches the lower wall when c approaches γ_1. In phase space, as c approaches the maximum wave speed $\gamma_1 \simeq 1.9099$, a cusp is formed at $(q,p)=(-H,0)$ on the homoclinic orbit. This is also true for mode-1 solitary wave of

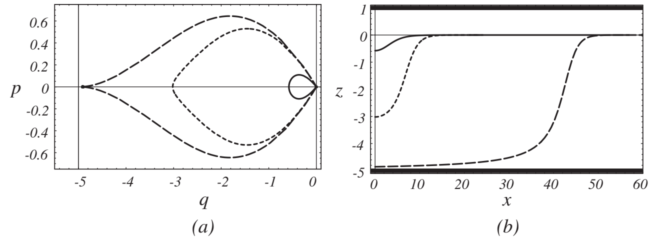

FIG. 4. (a) Homoclinic orbits in phase space $(q,p)\equiv(\zeta,\zeta_x)$ for mode-1 solitary waves of $c=0.8$ (—), 1.6 (- - - -), and 1.9 (— —) for $N=0$ and $H=5$. (b) The corresponding mode-1 solitary wave profiles of $a=-0.5765$, -3.0188, -4.8546, respectively. In this paper, since the solitary wave is symmetric about $x=0$, only a half of the solitary wave profile is shown.

maximum amplitude for the case of linear-linear density profile, as described in the Sec. III B. To determine whether such large amplitude internal waves can be observed in reality, their stability characteristics need to be examined.

The relationship between wave amplitude and wave speed for mode-1 solitary waves is shown in Fig. 5(a). It can be seen that for small amplitude waves, the wave speed c increases almost linearly with the wave amplitude a, but it does at a slower rate as the wave amplitude increases further. An approximate linear relationship between wave amplitude and wave speed was also found numerically by Grue *et al.*[13] up to $|a|\simeq 1.25$ in their computation for $H=4.13$ and was confirmed with their laboratory experiment. Beyond this amplitude, the observed solitary waves suffered from local wave breaking and no attempts were made to compute solitary wave solutions numerically. The wave amplitude of $|a|\simeq 1.25$ is much smaller than the maximum wave amplitude of $|a|=H(=4.13)$ that the present theory predicts and, therefore, it is not so surprising to find the linear relationship between c and a in their computation for $|a|<1.25$.

As the amplitude $|a|$ approaches its maximum value of H, mode-1 solitary waves become wider and wider, which can be seen from Fig. 5(b) for the half-width of the solitary wave, $\lambda_{1/2}$, defined by $\zeta(\lambda_{1/2})=a/2$. The wave speed and the half-width of mode-1 solitary waves increase with wave amplitude in a manner similar to that for solitary waves in a system of two constant density layers. For $H=5$, the half-width has a minimum of $\lambda_{\min}\simeq 3.676$ for $a\simeq -0.798$ (or $c\simeq 0.879$). As H decreases, the wave amplitude corresponding to the minimum wavelength decreases. For wave amplitudes close to the amplitude of minimum width, the long wave model becomes less valid, but it is expected to become in much better agreement with the original Euler equations as the wave amplitude increases, as noted for internal solitary waves in a two-layer system of constant densities.[11] The numerical result of Grue *et al.*[13] for $H=4.13$ showed no broadening of solitary waves up to $|a|\simeq 0.8$ although their laboratory experiment revealed significant broadening of solitary waves for $|a|>0.8$. We remark that the observed broadening in the laboratory experiment for relatively small wave amplitudes seems to be different from the broadening of large amplitude waves shown in Fig. 5(b). The observed broadening was attributed to local wave breaking that occurs when the local fluid velocity is close to or exceeds the wave speed. A description of time-dependent wave breaking is beyond the scope of this paper, but it would be interesting to examine the stability characteristics of large amplitude solitary waves that we describe in this paper.

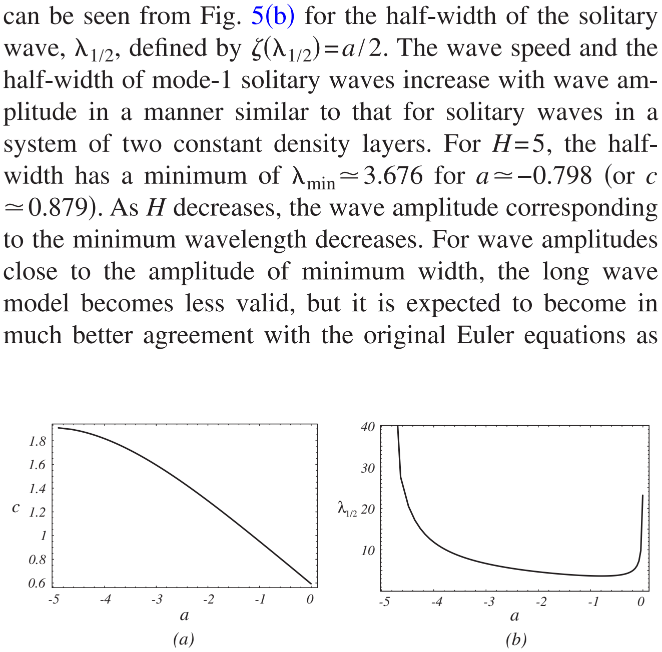

FIG. 5. (a) Solitary wave speed c vs wave amplitude a for mode-1 solitary waves for $N=0$ and $H=5$. (b) Half-width λ vs wave amplitude a.

For the case of constant-linear density profile, the stream function $\psi_i(x,z)$ induced by internal solitary waves is given by Eq. (8). For the lower layer with $N=0$, the expression for ψ_2 can be further reduced to

$$\psi_2(x,z)=-\frac{c(H+z)\zeta}{H+\zeta}+\frac{(H+z)}{6}\left(\frac{c\zeta}{H+\zeta}\right)_{xx}\times[(H+z)^2-(H+\zeta)^2]. \tag{21}$$

Figure 6 shows streamlines of Ψ=constant for solitary waves of $c=0.7$, 1.2, and 1.85, where Ψ is the total stream function defined by Eq. (2). When the solitary wave speed (or amplitude) is greater than a critical value, a recirculating eddy, or a set of closed streamlines emerges in the upper layer, as shown in Figs. 6(b) and 6(c). This is not possible for a two-layer system of constant densities unless a background shear is present.[22] To find a critical wave speed at which a recirculating eddy emerges in the upper layer, we look for a condition for a stagnation point to appear on the upper wall at $(x,z)=(0,1)$. As the wave speed increases beyond the critical wave speed, this stagnation point splits into two stagnation points located symmetrically about $x=0$ so that a recirculating eddy is formed. Since the total horizontal velocity at the center of the upper wall, $U_1(x,z)=\Psi_{1z}$ at $(x,z)=(0,1)$, is expressed by

$$U_1(0,1)=c+\frac{1}{2}\csc\left(\frac{a-1}{c}\right)\left[-2a-\left\{c-(a-1)\cot\left(\frac{a-1}{c}\right)\right\}\times\left\{c-a\cot\left(\frac{a-1}{c}\right)\right\}\zeta''(0)\right], \tag{22}$$

we can find numerically the critical wave speed $c_{\rm cr}$ from $U_1(0,1)=0$. At this critical wave speed, the local fluid velocity at $(x,z)=(0,1)$, $u_1=\psi_{1z}(0,1)$, induced by the internal solitary wave has the same magnitude as the wave speed c, but opposite sign. After using $\zeta''(0)=-C(a)/A(a)$ from Eq. (10) with $\zeta(0)=a$ and $\zeta'(0)=0$ and the relationship between c and a shown in Fig. 5(a), we can find $c_{\rm cr}\simeq 0.73$ for $H=2$ and $c_{\rm cr}\simeq 0.925$ for $H=5$. The corresponding critical wave amplitudes are $a_{\rm cr}\simeq -0.656$ and $a_{\rm cr}\simeq -0.926$ for $H=2$ and 5, respectively. For $H=4.13$, the critical wave amplitude is found $a_{\rm cr}\simeq -0.886$ that is comparable to $a_{\rm cr}\simeq -0.855$ computed numerically by Grue *et al.*[13] This difference of about 3% between the long wave theory and their numerical value

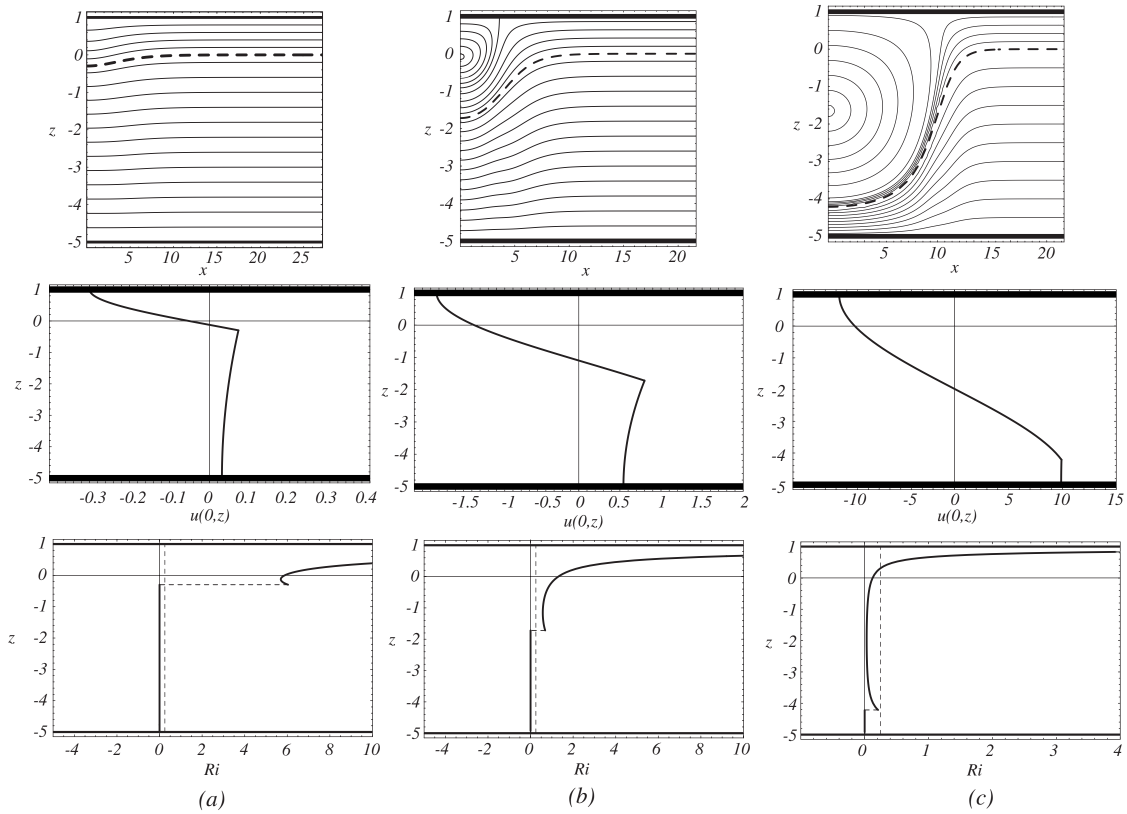

FIG. 6. Streamlines of Ψ=constant (top), the induced horizontal velocity $u=\psi_z$ at $x=0$ (middle), and the Richardson number Ri at $x=0$ (bottom) for mode-1 solitary waves for $N=0$ and $H=5$: (a) Wave speed, $c=0.7$; (b) $c=1.2$; (c) $c=1.85$. The corresponding wave amplitudes are $|a|\simeq 0.298$, 1.719, and 4.212, respectively. Notice that the dashed lines in the plots for the Richardson number indicate the critical Richardson number of 0.25.

is not clear, but the two values compare surprisingly well when considering that the critical wave amplitude is not so different from the amplitude for the minimum wavelength ($a\simeq -0.725$) for which the long wave model is expected to compare less favorably with the Euler equations.

Figure 6 also shows the vertical variation of the horizontal velocity induced by mode-1 solitary wave along the maximum displacement of the interface and the Richardson number Ri defined by

$$\mathrm{Ri}^2 = N_i^2/(u_{i,z})^2. \qquad (23)$$

Notice that the induced horizontal velocity u_i defined by $u_i \equiv \psi_{i,z}$ vanishes at a point on the axis of symmetry at $x=0$ in the upper layer, as predicted by linear theory, although the wave speed c needs to be added to u_i to obtain the total velocity. The horizontal velocity variation in the vertical direction is, in fact, indistinguishable from the numerical solution of Grue *et al.*[13] to graphical accuracy.

For case 1, the Richardson number for the upper layer is given by $\mathrm{Ri}=1/(u_{i,z})^2$ and that for the lower layer of constant density is $\mathrm{Ri}=0$. It is well known, from linear stability analysis, that a vertically sheared parallel flow in a stably stratified fluid could be unstable when the Richardson number is less than the critical Richardson number of 0.25. We remark that this criterion is a necessary condition for shear instability while it is a sufficient condition for stability. In Fig. 6, for $c=1.85$, it is observed that the local Richardson number computed using Eq. (23) becomes less than 0.25 inside the recirculating eddy. The flow induced by a solitary wave is not strictly parallel, but the variation of the horizontal velocity in the horizontal direction is negligible for long waves so that the Richardson number criterion can be used. The solitary wave shown in Fig. 6(c) could therefore be locally unstable although the local Richardson number is found experimentally to be much lower than 0.25 when periodic internal waves become unstable by the Kelvin–Helmholtz instability.[23]

The wave amplitude ($a_{0.25}$) for which the minimum Richardson number in the upper layer becomes equal to 0.25 is computed numerically and is compared in Fig. 7 with the critical wave amplitude (a_{cr}) beyond which a recirculating

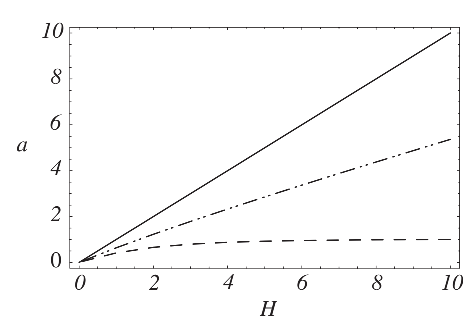

FIG. 7. Critical wave amplitude (a_{cr}, – –) beyond which a recirculating eddy appears is compared to wave amplitude of Ri=0.25 ($a_{0.25}$) (— – — –) and the maximum amplitude $a_{\max}=H$ (—) for varying H.

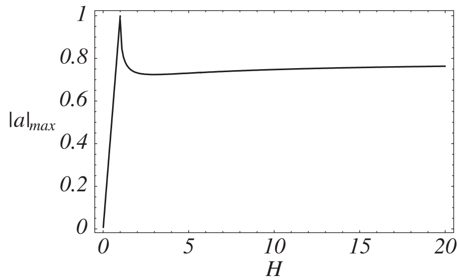

FIG. 8. The maximum amplitude of mode-2 solitary waves vs the depth ratio H for $N=0$.

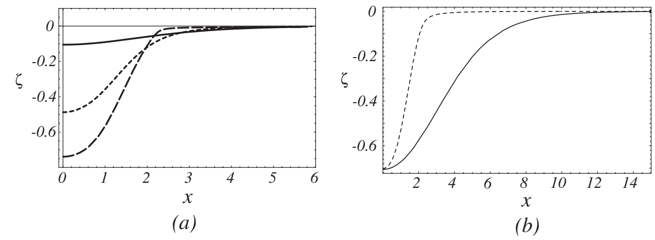

FIG. 9. (a) Mode 2 solitary wave profiles for $N=0$ and $H=5$. The wave speeds are $c=0.225$ (——), 0.28 (- - -), and 0.318 (– – –), and the corresponding amplitudes are approximately $a=-0.105$, -0.484, and -0.734, respectively. (b) Comparison of solitary waves of mode 1 (——) and mode 2 (- - - -) for wave amplitude $a=-0.7$. The corresponding wave speeds are $c=0.846$ and $c=0.313$ for modes 1 and 2, respectively.

eddy first appears. Notice that a_{cr} is always smaller than $a_{0.25}$. For a fixed depth ratio, unless there is an instability mechanism other than shear instability, a recirculating eddy in the upper layer appears for $|a|>a_{cr}$ until $|a|$ exceeds $a_{0.25}$. For $|a|>a_{0.25}$, the solitary waves could become unstable.

B. Mode-2 solitary waves

The behavior of mode-2 solitary wave solutions depends primarily on the depth ratio H and the following two ranges of H will be considered: $H\leq 1$ and $H>1$. When the thickness of the lower layer of constant density is smaller than that of the upper layer of linear density stratification ($H\leq 1$), mode-2 solitary waves of negative polarity of $-H\leq a<0$ exist and the solitary wave of maximum amplitude reaches the lower wall. On the other hand, when the lower layer of constant density is deeper ($H>1$), the maximum solitary wave amplitude is always smaller than the thickness of the lower layer so that $-H<a_{\max}\leq a<0$. As shown in Fig. 8, the maximum amplitude approaches $a_{\max}\simeq -0.791$ for large H. The corresponding wave speed ranges are $c_2\leq c\leq \gamma_1/2<\gamma_2$ and $c_2\leq c\leq \gamma_2(=1/\pi)$ for $H\leq 1$ and $H>1$, respectively, where c_2 is mode-2 linear wave speed and γ_1 and γ_2 can be computed from Eqs. (20) and (19), respectively.

For $H=5$, the profiles of mode-2 solitary waves for three different wave amplitudes (or wave speeds) are shown in Fig. 9(a). Unlike mode-1 solitary waves, the half-width of mode-2 solitary waves decreases slightly as the wave amplitude increases. As can be seen in Fig. 9(b), mode-2 solitary wave is narrower and travels slower when compared to mode-1 solitary wave of same amplitude. On the other hand, for $H\leq 1$, the width of mode-2 solitary waves increases as a approaches $-H$.

A recirculating eddy appears in the upper layer of linear stratification when mode-2 solitary wave speed (or wave amplitude) is greater than a critical value. While a monopole-type eddy is observed with mode-1 solitary waves, a dipole-type eddy is accompanied by mode-2 solitary waves. Figure 10 shows streamlines inside a recirculating eddy for a mode-2 solitary wave of $c=0.28$ for three different values of H. It is interesting to notice that the flow pattern inside a recirculating eddy can vary depending on the depth ratio H. For small H, the recirculating eddy has a normal dipole structure, as depicted in Fig. 10(a), but, for $H>1.357$, its interior flow configuration undergoes a bifurcation and turns into a more complicated pattern, as shown in Fig. 10(b). As H increases further, a normal dipole structure reappears. Stability characteristics of recirculating eddies of different flow patterns are of interest, but cannot be determined from the present steady long wave theory. For a fixed wave amplitude, the Richardson number inside mode-2 eddy is found smaller compared to that inside mode-1 eddy and, therefore, mode-2 solitary wave seems to be more susceptible to shear instability.

IV. CASE 2: LINEAR-LINEAR DENSITY PROFILE

We now consider the case of a piecewise linear density profile and, in addition to the depth ratio H, the ratio of buoyancy frequencies N is another physical parameter. As shown in Appendix B, it is found that the polarity of solitary waves depends only on N, but is independent of the depth ratio H. Solitary waves are always of depression for $N<1$ (when the density gradient of the lower layer is less than that of the upper layer) and of elevation for $N>1$. This implies that solitary waves always point into the layer of smaller density gradient, which is consistent with the previous observation for the linear-constant density profile case where solitary waves point into the lower layer of zero density gradient. This observation is valid for both mode-1 and mode-2 solitary waves. For $N=1$, there is no jump in density gradient and, therefore, no solitary waves exist; for $N=0$, the results for case 1 can be recovered.

A. Mode-1 solitary waves

For case 2, mode-1 solitary wave solutions exist in the following speed ranges

$$c_1<c<\gamma_1 \quad \text{for } N<1, \quad c_1<c<N\gamma_1 \quad \text{for } N>1, \qquad (24)$$

where c_1 is the fastest linear long wave speed satisfying the linear dispersion relation given by Eq. (18) and $\gamma_1=(1+H)/\pi$ is given by Eq. (20). These admissible ranges of c are illustrated in Fig. 11 for $H=5$, 1, and 0.5. The lower boundary of the shaded region represents the linear long wave speed given by Eq. (18). For fixed H, the maximum wave speed (or the upper boundary of the shaded region in Fig. 11) is independent of N for $N<1$, while it is a linear function of N for $N>1$. As the wave speed c approaches its maximum value γ_1 or $N\gamma_1$, the solitary wave reaches the

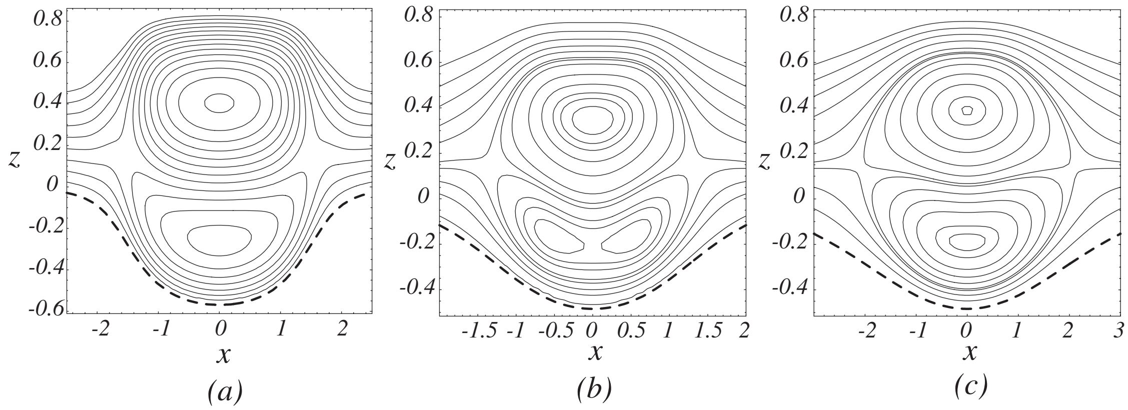

FIG. 10. Close-up view of streamlines for $N=0$ and $c=0.28$ for three different depth ratios: (a) $H=1$, (b) $H=5$, and (c) $H=20$.

lower or upper wall, for $N<1$ and $N>1$, respectively. It can be noticed from Fig. 11(a) that, for large H, the range of admissible wave speed between the minimum and maximum speeds is very narrow for $N>1$ and, therefore, the wave speed is almost independent of the wave amplitude a, where $0<a\leq 1$. On the other hand, for small H, the range of wave speed is relatively narrow for $N<1$.

Figure 12 shows the streamlines, the induced horizontal velocities at the maximum interfacial displacement, and the variation of the Richardson number in the vertical direction at $x=0$ for solitary waves of wave speed $c=1.6$, 1.75, and 1.908 for $H=5$ and $N=0.8$. The wave characteristics of mode-1 solitary waves for case 2 are found very similar to those for case 1 with $N=0$. A recirculating eddy can be observed when the wave speed (or the wave amplitude) is greater than a critical value, as noted previously. The Richardson number is greater than 0.25 everywhere along the axis of symmetry (at $x=0$) for $c=1.6$ and 1.75, while it becomes less than 0.25 for $c=1.908$.

B. Mode-2 solitary waves

For $N=0$, it was found in case 1 that mode-2 solitary waves of negative polarity exist up to a maximum wave amplitude that is equal to or smaller than the thickness of the lower layer for $H<1$ and $H>1$, respectively. For nonzero N, there are two special values of N for which no solitary wave solutions can be found: $N=1$ and $N=1/H$. The former ($N=1$) represents a single layer system of uniform linear stratification for which no solitary wave solutions of any mode are known to exist since the problem becomes linear. On the other hand, mode-1 solitary wave solution exists even for $N=1/H$.

The speed range for which mode-2 solitary waves exist is shown in Fig. 13 for $H=5$, 1, and 0.3. Notice that, for some values of N, a narrow range of speed is allowed for mode-2 solitary waves, in particular, for $H=5$. To describe mode-2 solitary waves for varying N in detail, the case of $H>1$ for which the thickness of the lower layer is greater than that of the upper layer is considered first and the results for $H<1$ will be summarized later.

For small N for which the buoyancy frequency of the lower layer is smaller than that of the upper layer, solitary waves of depression exist over a speed range of $c_2<c<\gamma_2(=1/\pi)$ for $N<1/H$, as shown in Fig. 13(a). For this range of N, while the maximum wave speed is independent of N, the maximum wave amplitude is a function of N and is always smaller than the thickness of the lower layer. In Fig. 14(a) with $H=5$ and $N=0.1$, the solitary wave profiles are shown for three different wave speeds of $c=0.23$, 0.26, and 0.317. Unlike mode-1 waves, the width of mode-2 solitary waves decreases slightly as the amplitude increases. A similar observation has been made for the case of $N=0$.

For $1/H<N<1$, mode-2 solitary waves of depression exist over a speed range of $c_2\leq c\leq N\gamma_1/(1+N)$. As shown in Fig. 14(b), the width of the solitary waves increases with the wave speed (or the wave amplitude), which has not been observed for small $N(<H^{-1})$. By tracking the location of a singularity of the right-hand side of the system given by Eq.

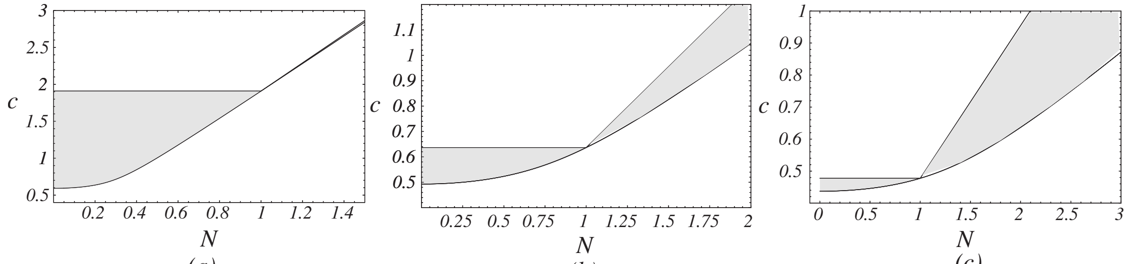

FIG. 11. Admissible wave speed (shaded region) c vs N for mode-1 solitary waves to exist for case 2: (a) $H=5$; (b) $H=1$; (c) $H=0.5$.

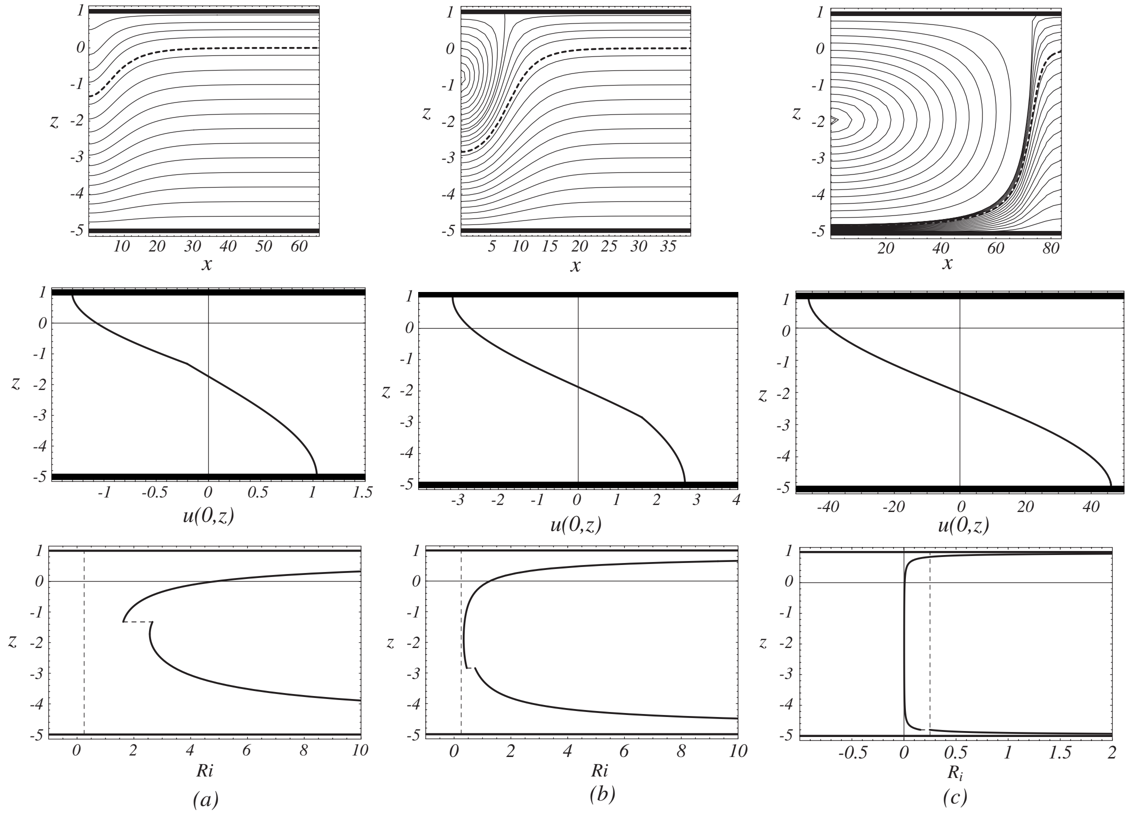

FIG. 12. Streamlines of Ψ=constant (top), the induced horizontal velocity $u=\psi_z$ at $x=0$ (middle), and the Richardson number Ri at $x=0$ (bottom) for mode-1 solitary waves for $H=5$ and $N=0.8$: (a) Wave speed $c=1.6$; (b) $c=1.75$; (c) $c=1.908$.

(14) located outside a homoclinic orbit, the maximum wave amplitude is found to be $|a|_{\max}=(1+NH)/(1+N)<H$ at which the singular point touches the homoclinic orbit.

For $N>1$, the buoyancy frequency in the upper layer is smaller and, therefore, mode-2 solitary waves are of elevation. The range of wave speed lies in $c_2 \le c \le N\gamma_1/2$. As can be seen from Fig. 14(c), the width of the solitary waves increases as the wave amplitude increases and the solitary wave of maximum amplitude reaches the upper wall.

When the thickness of the lower layer is equal to or smaller than that of the upper layer ($H=1$ or $H<1$), the ranges of wave speed and wave amplitude are summarized in Table I.

Although the solution behavior for mode-2 solitary waves is complicated, our findings for mode-2 solitary waves can be summarized as follows. First, the polarity of solitary waves is determined by N: Solitary waves of depression for $N<1$ and of elevation for $N>1$. Second, the solitary wave of maximum amplitude can reach the upper or lower boundary when the solitary wave points toward the thinner layer; otherwise, the maximum amplitude is smaller than the thickness of the deeper layer. Lastly, the width of mode-2 solitary waves does not necessarily increase as the wave amplitude increases.

V. CONCLUSION

We have studied large amplitude internal solitary waves for a two-layer system of linear stratification using a strongly nonlinear asymptotic model derived under the long wave approximation with no smallness assumption on wave amplitude. Two layers have different constant buoyancy (Brunt–Väisälä) frequencies, but the density is continuous across the interface. For linear-constant and linear-linear density pro-

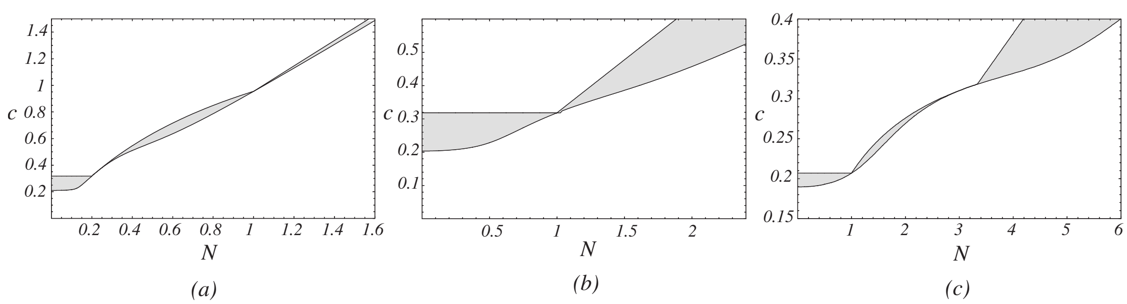

FIG. 13. Admissible wave speed c vs N for the second mode: (a) $H=5$; (b) $H=1$; (c) $H=0.3$.

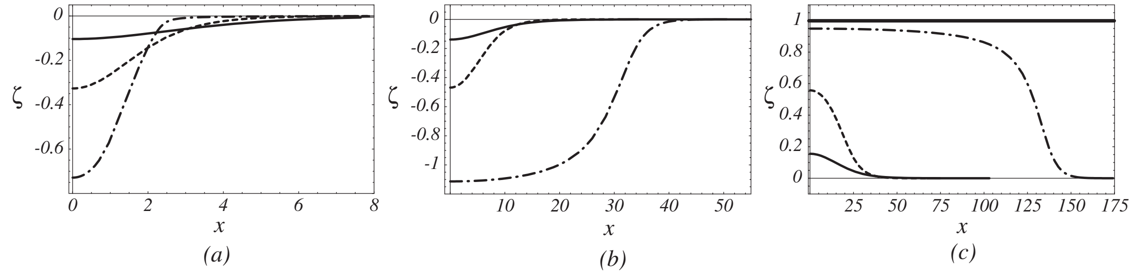

FIG. 14. Mode-2 solitary wave profiles for $H=5$: (a) $N=0.1$ and $c=0.23$, 0.26, 0.317; (b) $N=0.6$, $c=0.65$, 0.68, 0.715; (c) $N=1.4$, $c=1.315$, 1.33, 1.3368.

files, both mode-1 and mode-2 solitary wave solutions are described in detail over the entire physical parameter space of depth and buoyancy frequency ratios.

Regardless of the depth ratio, it is found that the internal solitary waves always point to the layer of smaller buoyancy frequency. For a system of two constant density layers, the polarity of internal solitary waves is determined by the density and depth ratios. For fixed depth and buoyancy frequency ratios, a recirculating eddy appears at the wave crest when the wave amplitude exceeds a critical value. Mode-1 internal solitary waves become wider as the wave amplitude increases which is not necessarily true for mode-2 internal solitary waves. The solitary wave of maximum amplitude can reach either the upper or lower wall although large amplitude solitary waves might be unstable since the Richardson number inside the recirculating region could become less than $\frac{1}{4}$ (according to the Richardson number criterion for shear instability).

Even though the results presented in this paper are based on the long wave model, it is found that they show good agreement with the fully nonlinear numerical results of Grue *et al.*[13] for mode-1 solitary waves. Keeping in mind that the reduced gravity can be assumed to be small for oceanic applications, the characteristic horizontal length scale increases as the wave amplitude increases and, therefore, the long wave solutions for large amplitude internal solitary waves are expected to be a good approximation to the fully nonlinear solutions of the Euler equations, as noticed for a two-layer system of constant densities.[11] For continuously stratified fluids, using a singular perturbation technique, Akylas and Grimshaw[24] computed mode-2 internal solitary waves with oscillatory tails excited in resonance with mode-1 periodic waves whose phase velocity is the same as mode-2 long wave speed. Since we consider a long wave model with zero boundary conditions at both infinities, the existence of mode-2 solitary waves with oscillatory tails for the present two-layer system cannot be addressed and it is required to solve the Euler equations to find such solitary wave solutions.

For a system of two constant density layers, the solitary wave solutions of the inviscid model have been known to suffer from the Kelvin–Helmholtz instability since only continuity of normal velocity is imposed to derive the model and a jump in tangential velocity is induced when the interface is deformed.[25,26] Here, the solitary wave solutions are obtained with imposing continuity of both tangential and normal velocities, but might still be locally unstable for large wave amplitudes when the Richardson number criterion is applied at the location of maximum interfacial displacement. It would be interesting to study the dynamics of both stable and unstable solitary waves, but the present steady formulation needs to be greatly modified.

TABLE I. Wave speed c and wave amplitude a of mode-2 solitary waves for varying N: (a) $H>1$; (b) $H=1$; (c) $H<1$. Here, a_{num} is the maximum wave amplitude that can be computed only numerically and no explicit expression has been found.

(a) $H>1$	$0<N<1/H$	$1/H<N<1$	$1<N$
c	$c_2\le c<1/\pi$	$c_2\le c\le N\gamma_1/(1+N)$	$c_2\le c\le N\gamma_1/2$
a	$a_{\mathrm{num}}\le a\le 0$	$(1-NH)/(1+N)\le a\le 0$	$0\le a\le 1$
(b) $H=1$		$0<N<1$	$1<N$
c		$c_2\le c\le 1/\pi$	$c_2\le c\le N/\pi$
a		$-1\le a\le 0$	$0\le a\le 1$
(c) $H<1$	$0<N<1$	$1<N<1/H$	$1/H<N$
c	$c_2\le c\le \gamma_1/2$	$c_2\le c\le N\gamma_1/(1+N)$	$c_2\le c\le NH/\pi$
a	$-H\le a\le 0$	$0\le a\le (1-NH)/(1+N)$	$0\le a\le a_{\mathrm{num}}$

ACKNOWLEDGMENTS

The authors gratefully acknowledge support from the National Science Foundation through Grant No. DMS-0620832 and the Office of Naval Research through Grant No. N00014-08-1-0377.

APPENDIX A: BOUNDARY CONDITIONS: PRESSURE CONTINUITY VERSUS VELOCITY CONTINUITY

The pressure at the interface P_i is given, from the steady Bernoulli equation,[15] by

$$P_i = -\tfrac{1}{2}(1+\zeta_x^2)(c+\psi_{i,z})^2 - \rho_i g\zeta + \tfrac{1}{2}c^2, \tag{A1}$$

where the kinematic boundary condition (5) has been used to express $\psi_{i,x}$ in terms of $\psi_{i,z}$, and both $\psi_{i,z}$ and ρ_i are evaluated at $z=\zeta$. Then, the pressure jump, $\Delta P \equiv P_1 - P_2$, is given by

$$\Delta P = -\tfrac{1}{2}(1+\zeta_x^2)(2c+\psi_{1,z}+\psi_{2,z})(\psi_{1,z}-\psi_{2,z}) - (\rho_1-\rho_2)g\zeta. \tag{A2}$$

In the presence of density jump ($\rho_1 \neq \rho_2$), when continuity of pressure ($\Delta P=0$) is imposed at the interface, the horizontal velocity (and, therefore, the tangential velocity) is discontinuous across the interface, as expected, and the interface can be considered a vortex sheet. On the other hand, when the density is continuous across the interface ($\rho_1=\rho_2$), continuity of pressure gives

$$\Delta P = (2c + \psi_{1,z} + \psi_{2,z})(\psi_{1,z} - \psi_{2,z}) = 0, \tag{A3}$$

which yields not only a physical solution satisfying continuity of horizontal velocity ($\psi_{1,z}-\psi_{2,z}=0$) across the interface but also a spurious nonphysical solution ($2c+\psi_{1,z}+\psi_{2,z}=0$) for which continuity of tangential velocity is violated. On the other hand, when continuity of horizontal velocity ($\psi_{1,z}=\psi_{2,z}$) is imposed at the interface, continuity of pressure is always satisfied.

Furthermore, when the DJL equation is solved using asymptotic expansion, the two different boundary conditions make a more significant difference even when $\rho_1=\rho_2$: continuity of pressure whose expression is valid only to $O(H_i^2/\lambda^2)$ cannot be written as Eq. (A3) due to the truncation of higher-order terms and, therefore, continuity of tangential velocity is not guaranteed. This explains why the coefficients of the equation for ζ in Voronocich[15] resulting from pressure continuity is different from those of Eq. (10) in this paper.

APPENDIX B: POLARITY OF SOLITARY WAVES

In order to show that the polarity of internal solitary waves in a linearly stratified two-layer system depends solely on the buoyancy frequency ratio N, we study the system given by Eq. (14) when the wave speed c is close to the linear wave speed c_i given by Eq. (18). For $c=c_i$, notice that the Jacobian of the system at the origin of phase space, $(q,p)=(0,0)$, has the form of

$$J = \begin{pmatrix} 0 & 1 \\ 0 & 0 \end{pmatrix}$$

with double zero eigenvalues, for which a bifurcation known as Takens–Bogdanov bifurcation[27] can occur. One scenario for this bifurcation is that the origin splits into a saddle point and an elliptic point enclosed by a homoclinic orbit representing a solitary wave solution. Therefore, the polarity of the solitary wave depends on the relative position of the elliptic point with respect to the origin.

We first expand the right-hand side of system (14) about the origin $(q,p)=(0,0)$ up to quadratic order in q and p to obtain

$$\dot{q} = p, \quad \dot{p} = A_1 q + A_2 q^2 + A_3 p^2, \tag{B1}$$

where A_i are constants depending on the parameters c, N, and H with $A_1=0$ for $c=c_i$. In this reduced system, the fixed points are given by $(0,0)$ and $(-A_1/A_2,0)$ and it can be shown that the second fixed point is an elliptic point since its eigenvalues are purely imaginary. By assuming $c=c_i+\epsilon$ with $0<\epsilon\ll 1$ and expanding the expression of $-A_1/A_2$ up to first order in ϵ, we obtain

$$-\frac{A_1}{A_2} \sim \frac{\epsilon}{2c_i} \frac{HN^2\csc^2(HN/c_i) + \csc^2(1/c_i)}{N^2\csc^2(HN/c_i) - \csc^2(1/c_i)}. \tag{B2}$$

The numerator of Eq. (B2) is always positive and the sign of $-A_1/A_2$ (or the polarity) is therefore determined by the denominator. In fact, it is found numerically that $-A_1/A_2<0$ for $N<1$ and $-A_1/A_2>0$ otherwise. This implies that the elliptic fixed point is located on the negative q axis for $N<1$ and on the positive q-axis for $N>1$. Thus, it can be concluded that the polarity of solitary waves depends only on N and the solitary waves always point to a layer of smaller buoyancy frequency.

[1] M. K. Dubreil-Jacotin, "Sur les théoremes d'existence relatifs aux ondes permanentes pérodiques à deux dimensions dans les liquides hétérogènes," J. Math. Pures Appl. **16**, 43 (1937).
[2] R. R. Long, "Some aspects of the flow of stratified fluids," Tellus **5**, 42 (1953).
[3] K.-K. Tung, T.-F. Chan, and T. Kubota, "Large amplitude internal waves of permanent form," Stud. Appl. Math. **66**, 1 (1982).
[4] B. Turkington, A. Eydeland, and S. Wang, "A computational method for solitary waves in a continuously stratified fluid," Stud. Appl. Math. **85**, 93 (1991).
[5] D. J. Brown and D. R. Christie, "Fully nonlinear solitary waves in continuously stratified incompressible fluids," Phys. Fluids **10**, 2569 (1998).
[6] M. Stastna and K. G. Lamb, "Large fully nonlinear internal solitary waves: The effect of background current," Phys. Fluids **14**, 2987 (2002).
[7] C. G. Koop and G. Butler, "An investigation of internal solitary waves in a two-fluid system," J. Fluid Mech. **112**, 225 (1981).
[8] H. Michallet and E. Barthélemy, "Experimental study of interfacial solitary waves," J. Fluid Mech. **366**, 159 (1998).
[9] M. Miyata, "Long internal waves of large amplitude," in Proceedings of the IUTAM Symposium on Nonlinear Water Waves, edited by H. Horikawa and H. Maruo (Springer-Verlag, New York, 1988), p. 399.
[10] W. Choi and R. Camassa, "Fully nonlinear internal waves in a two-fluid system," J. Fluid Mech. **396**, 1 (1999).
[11] R. Camassa, W. Choi, H. Michallet, P.-O. Rusas, and J. K. Sveen, "On the realm of validity of strongly nonlinear asymptotic approximations for internal waves," J. Fluid Mech. **549**, 1 (2006).
[12] J. Grue, A. Jensen, P.-O. Rusas, and J. K. Sveen, "Properties of large-amplitude internal waves," J. Fluid Mech. **380**, 257 (1999).
[13] J. Grue, A. Jensen, P.-O. Rusas, and J. K. Sveen, "Breaking and broadening of internal solitary waves," J. Fluid Mech. **413**, 181 (2000).
[14] D. Fructus and J. Grue, "Fully nonlinear solitary waves in a layered stratified fluid," J. Fluid Mech. **505**, 323 (2004).
[15] A. G. Voronovich, "Strong solitary internal waves in a 2.5-layer model," J. Fluid Mech. **474**, 85 (2003).
[16] T. P. Stanton and L. A. Ostrovsky, "Observation of highly nonlinear internal solitons over the continental shelf," Geophys. Res. Lett. **25**, 2695 (1998).
[17] S. R. Ramp, T. Y. Tang, T. F. Duda, J. F. Lynch, A. K. Liu, C.-S. Chiu, F. L. Bahr, H. R. Kim, and Y. J. Yang, "Internal solitons in the Northeastern South China Sea. Part. I: Sources and deep water propagation," IEEE J. Ocean. Eng. **29**, 1157 (2004).
[18] R. E. Davis and A. Acrivos, "Solitary internal waves in deep water," J. Fluid Mech. **29**, 593 (1967).
[19] A. P. Stamp and M. Jacka, "Deep-water internal solitary waves," J. Fluid Mech. **305**, 347 (1995).
[20] P. Rusas and J. Grue, "Solitary waves and conjugate flows in a three-layer fluid," Eur. J. Mech. B/Fluids **21**, 185 (2002).
[21] H. Michallet and F. Dias, "Numerical study of generalized interfacial solitary waves," Phys. Fluids **11**, 1502 (1999).
[22] W. Choi, "The effect of a background shear current on large amplitude internal solitary waves," Phys. Fluids **18**, 036601 (2006).
[23] C. D. Troy and J. R. Koseff, "The instability and breaking of long internal waves," J. Fluid Mech. **543**, 107 (2005).
[24] T. R. Akylas and R. H. J. Grimshaw, "Solitary internal waves with oscillatory tails," J. Fluid Mech. **242**, 279 (1992).
[25] T.-C. Jo and W. Choi, "Dynamics of strongly nonlinear solitary waves in shallow water," Stud. Appl. Math. **109**, 205 (2002).
[26] T.-C. Jo and W. Choi, "On stabilizing the strongly nonlinear internal wave model," Stud. Appl. Math. **120**, 65 (2008).
[27] J. Guckenheimer and P. Holmes, *Nonlinear Oscillations, Dynamical Systems, and Bifurcations of Vector Fields* (Springer-Verlag, New York, 1983).